Nucleation in supersaturated solutions of ^{3}He in ^{4}He at negative pressures

Montserrat Guilleumas, Martí Pi, and Manuel Barranco
Departament d'Estructura i Constituents de la Matèria, Facultat de Física, Universitat de Barcelona, E-08028 Barcelona, Spain

Dora M. Jezek
Departamento de Física, Facultad de Ciencias Exactas y Naturales, Universidad de Buenos Aires, RA-1428 Buenos Aires, Argentina

Jesús Navarro
Instituto de Física Corpuscular (Centre Mixt, Consejo Superior de Investigaciones Científicas, Universitat de València), Facultat de Física, E-46100 Burjassot, Spain
(Received 6 February 1995)

Depending on the ^{3}He concentration, thermal nucleation in ^{3}He-^{4}He supersaturated liquid mixtures at negative pressures may be originated either by bubble or by ^{3}He-rich drop formation. We have investigated this phenomenon within a density-functional approach, determining the regions in the pressure–^{3}He-concentration plane where bubbles or drops likely drive the nucleation process. As an illustrative example, we also give the homogeneous nucleation pressure corresponding to 50 and 100 mK temperature.

I. INTRODUCTION

Thermal nucleation in binary mixtures is receiving much attention[1,2] due to its importance in technical applications. Similar to the case of one-component systems, the frame for the theoretical understanding of this phenomenon has been provided for a long time by the classical nucleation theory. It makes use of the capillarity approximation, in which the free energy of a sharp-surface nucleus is written as the sum of a bulk and a surface term. Although this description can be safely used near the saturation line, it is certainly incorrect near the spinodal line, because here it predicts a nonvanishing nucleation barrier. The density-functional approach overcomes the shortcomings inherent in the capillarity approximation; moreover, it has been shown[3] that the effects of surface enrichment and curvature are also naturally included in such an approach.

Liquid helium at low temperatures has been considered as an useful tool for testing homogeneous nucleation theories,[2] mainly because near the absolute zero temperature (T) it can be prepared with a high degree of purity. However, helium is usually a mixture of ^{3}He and ^{4}He. In a recent work[4] we have used a density-functional approach to investigate thermal cavitation in solutions of ^{3}He in ^{4}He at negative pressures, low temperatures, and ^{3}He concentrations *below* saturation. We have shown that cavitation barriers are drastically reduced as compared to those corresponding to pure ^{4}He since the presence of Andreev states lowers the surface tension of the mixture. Bubble formation is therefore substantially enhanced, even at ^{3}He concentrations as small as 10^{-4} %.

Due to the miscibility gap existing in ^{3}He-^{4}He mixtures, an interesting process appears. For ^{3}He concentrations above saturation, it is also possible, even at negative pressures, that phase separation originates by nucleation of ^{3}He *drops* in the mixture (hereafter referred to as drop formation). Therefore, two nucleation mechanisms are present at negative pressures: drop and bubble formation, competing somewhere in the pressure–^{3}He-concentration plane. In both cases, there is a critical nucleation cluster size above which the system will undergo phase separation. The associated free energy defines the barrier height that determines which of these processes is more probable.

The aim of this work is to use the density-functional approach of Ref. 4 to describe the nucleation process at different pressures (P) and ^{3}He concentrations (x). It is worth emphasizing that both drop and bubble profiles are naturally obtained in this approach. This is especially useful in multicomponent systems, where the shape of the nucleation cluster configuration cannot be easily guessed.

The plan of this work is as follows. In Sec. II we review the capillarity model. In Sec. III we calculate the surface tension of the mixture-free ^{3}He interface along the saturation curve as a function of ^{3}He concentration, since this is a key ingredient in the capillarity model and experimentally known only at $P=0$. Detailed numerical results obtained within the density-functional approach are presented in Secs. IV, and Sec. V contains a brief summary.

II. CAPILLARITY MODEL

To have a rough idea about drop and bubble nucleation processes, it is convenient to start by considering

0163-1829/95/52(2)/1210(5)/$06.00

the simplest capillarity model. In this approach the nucleation barrier is written as a balance between surface and volume terms[5]

$$U(R) = SR^2 - VR^3, \tag{1}$$

where R is the radius of the nucleation cluster. In the case of bubbles

$$S = 4\pi\sigma_B, \quad V = \frac{4\pi}{3}\Delta P, \tag{2}$$

where σ_B refers to the surface tension of the mixture *free* surface, and ΔP is the pressure difference between the bubble and the bulk. It is assumed that the density inside the bubble is zero, so that $\Delta P = -P$ (recall that P is a negative quantity).

In the case of drops[6,7]

$$S = 4\pi\sigma_D, \quad V = \frac{4\pi}{3}\Delta\mu_3\rho_3, \tag{3}$$

where σ_D refers to the surface tension of the mixture-*pure* ^{3}He interface, $\Delta\mu_3$ is the difference between the chemical potential of ^{3}He in the mixture and of pure ^{3}He at the same pressure, and ρ_3 is the ^{3}He particle density in the pure phase. For ^{3}He-^{4}He mixtures, the capillarity approach cannot describe drops at pressures below the spinodal one of pure ^{3}He [about -3 atm (Refs. 8 and 9)].

The barrier height is determined by the maximum value of $U(R)$, which occurs at a size $R_{\max} = 2S/3V$, and is equal to

$$U_{\max} = \frac{4}{27}\frac{S^3}{V^2}. \tag{4}$$

This maximum height diverges at $\Delta P = 0$ for bubbles, and at $\Delta\mu_3 = 0$ for drops, which correspond to the respective saturation curves.

Neglecting prefactors entering the nucleation rate definition (see Sec. IV), at a given temperature, bubble and drop configurations have the same probability to be formed when the nucleation barrier maxima become equal. This equality defines a transition pressure P_t

$$|P_t| = \Delta\mu_3\ \rho_3\ \left(\frac{\sigma_B}{\sigma_D}\right)^{3/2}. \tag{5}$$

This equation implicitly defines a curve in the (P, x) plane. On the right of this line, drops rather than bubbles are formed, and the contrary happens on the left. To make a quantitative prediction the surface-tension values are needed. We shall first obtain these values from a density-functional calculation, and defer the discussion to Sec. IV.

III. SURFACE TENSION ALONG THE SATURATION CURVE

A density-functional approach for ^{3}He-^{4}He mixtures at zero temperature was proposed by Dalfovo and Stringari,[10,11] the parameters of which have been adjusted so as to reproduce some experimental data of pure ^{3}He and ^{4}He systems, and of the mixture. We have employed the same functional but with the parametrization of Ref. 4, where the original surface parameters have been slightly modified to reproduce more accurately the experimental surface tension of pure ^{4}He and that of the mixture-pure ^{3}He interfaces at saturation.

The surface tension of the mixture free surface has been studied in Ref. 4 as a function of x. We now proceed to obtain that of the mixture-pure ^{3}He interface along the saturation curve, which is the relevant one for ^{3}He drop formation. The saturation curve $P_{\rm sat}(x)$, i.e., the maximum solubility curve, is determined by the two-phase equilibrium conditions.[4]

The calculation follows a similar line as for the free surface case. Given a point on the saturation curve, the ^{3}He and ^{4}He particle density profiles $\rho_3(z)$ and $\rho_4(z)$ are obtained by solving the coupled Euler-Lagrange (EL) equations

$$\frac{\delta f}{\delta\rho_i} = \frac{\partial f}{\partial\rho_i} - \nabla\frac{\partial f}{\partial(\nabla\rho_i)} = \mu_i\ , \quad i = 3, 4\ , \tag{6}$$

where $f(\rho_3, \rho_4)$ is the free energy of the system and μ_i is the corresponding chemical potential. We impose the following boundary conditions. When $z \to \infty$ the densities $\rho_i(z)$ tend to values ρ_i such that $x = \rho_3/(\rho_3 + \rho_4)$ and $\rho^2\partial f/\partial\rho|_x = P$. When $z \to -\infty$ only pure ^{3}He at pressure P is present.

The surface tension is calculated as

$$\sigma = \int_{-\infty}^{\infty} dz\ [f(z) - \mu_3\rho_3(z) - \mu_4\rho_4(z) + P]\ . \tag{7}$$

The surface tension of the pure ^{3}He-mixture interface is displayed in Fig. 1 as a function of x. We have started at $x = 4\%$, which corresponds to a pressure close to the spinodal pressure of pure ^{3}He, and have stopped the calculations at a value of x which roughly corresponds

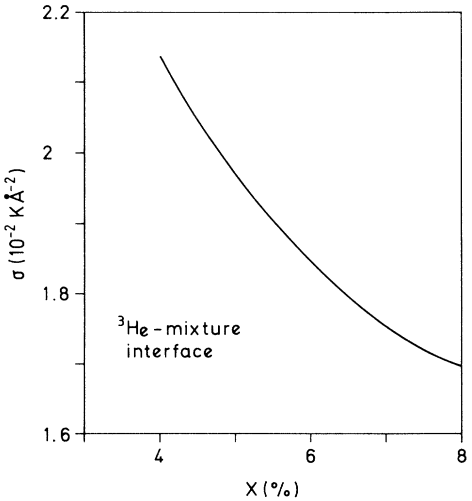

FIG. 1. Surface tension of the mixture-pure ^{3}He interface as a function of the ^{3}He concentration along the saturation curve.

to +3 atm. Above that value, the functional does not accurately reproduce the maximum ^{3}He solubility, see Ref. 11. Comparing the present results with those shown in Ref. 4, one can see that the surface tension of the mixture-pure ^{3}He interface is a factor of 10 smaller than that of the mixture free surface.

IV. DENSITY-FUNCTIONAL RESULTS

A. Particle density profiles for drops and bubbles

Particle density profiles $\rho_3(r)$ and $\rho_4(r)$ for the critical nucleus of total density $\rho(r) = \rho_3(r) + \rho_4(r)$, have been obtained by solving again the corresponding coupled EL equations. The boundary conditions are in this case $\rho_i'(0) = 0$, and $\rho_i(r \to \infty) = \rho_{im}$, where $\rho_m = \rho_{3m} + \rho_{4m}$ is the total density of the homogeneous metastable state at a given pressure, and $x = \rho_{3m}/\rho_m$ is the ^{3}He concentration. It is worth emphasizing that the same boundary conditions lead in general to two different configurations: one corresponding to a bubble with a ^{3}He enrichment at the surface, and another corresponding to a ^{3}He drop, both embedded in the mixture.

Typical profiles are shown in Figs. 2 and 3, for a pressure of -2.3 bar and concentrations $x = 5.5$ and 7.5%, respectively. For that pressure, the 5.5% concentration point lies closer to the saturation curve than the 7.5% point. As the *drop* nucleation barrier becomes infinite at this curve, the size of the critical cluster is larger (71 Å) in the former than in the latter (29 Å) case. Obviously, the variation in size for bubbles is not affected by crossing over the saturation line. In this example, the bubble radii are 17 and 15 Å for $x = 5.5$ and 7.5%, respectively. As a general trend, for given P and x, the size of the corresponding drop and bubble configuration differs most near saturation while they are similar when nearer the spinodal curve. It is worth noting that the pure ^{3}He-mixture interfacial region is rather independent of whether bubble or drop configurations are being formed (compare top and bottom panels in Figs. 2 and 3, for example).

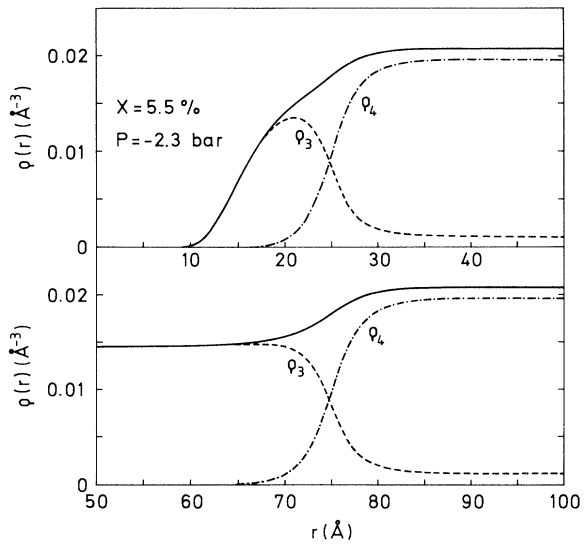

FIG. 2. Density profiles for $x = 5.5\%$ and $P = -2.3$ bar. Top panel, bubble configuration. Bottom panel, drop configuration. Dashed lines, ^{3}He densities; dashed-dotted lines, ^{4}He densities; solid lines, total densities.

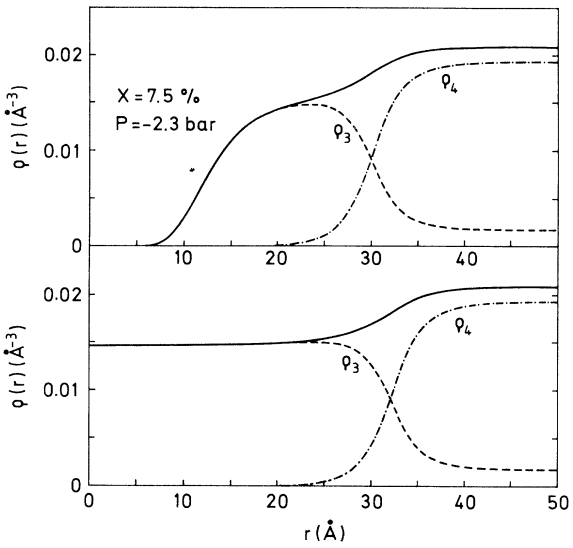

FIG. 3. Same as Fig. 2 for $x = 7.5\%$.

B. Barriers

The homogeneous, metastable state is separated from the stable one by a nucleation barrier, which may be overcome either by thermal fluctuations or by quantum tunneling at temperatures low enough.[5] The barrier height is determined by the free energy of the critical nucleus, which is such that with any further increase in size, it may continue to grow without any external intervention and trigger the phase separation.

The nucleation barrier height $\Delta\Omega$ is then obtained from the difference between the grand potential of the critical cluster and that of the homogeneous metastable state:

$$\Delta\Omega = \int d\vec{r}\,[f(\rho_3,\rho_4) - f(\rho_{3m},\rho_{4m}) - \mu_3(\rho_3 - \rho_{3m}) - \mu_4(\rho_4 - \rho_{4m})]\,. \tag{8}$$

For the configurations shown in Fig. 2, bubble nucleation is more favorable than drop nucleation: their barrier heights are 164 and 449 K, respectively. For the configurations shown in Fig. 3, the reverse situation is obtained: the barrier height for the drop is 71 K, whereas it is 123 K for the bubble. At the intermediate value $x = 6.54\%$ the barrier heights become equal.

In Fig. 4 we show the ^{3}He-drop nucleation barrier heights for different concentrations as a function of P. As expected, they diverge at saturation and vanish at spinodal values. The bubble barrier heights can be found in

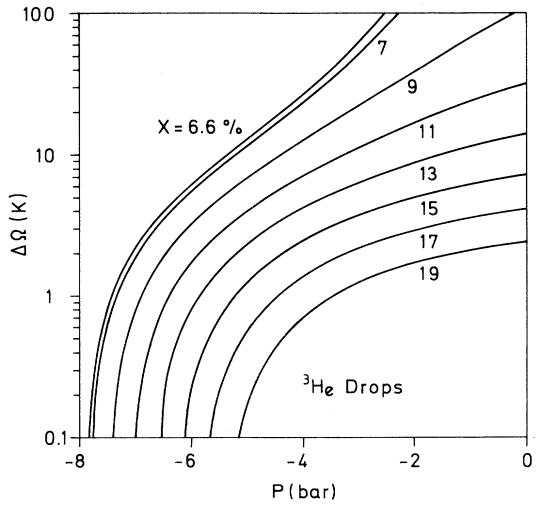

FIG. 4. Drop barrier heights (K) as functions of pressure (bar). From top to bottom, the curves correspond to x =6.6 (saturation), 7, 9, 11, 13, 15, 17, and 19%.

Ref. 4. As functions of P and x, the barriers $\Delta\Omega(P,x)$ define two surfaces that grow from zero at the spinodal line, cross each other at the transition pressure P_t line and finally diverge at the corresponding saturation pressures. It is interesting to notice that, since experimentally at very low temperatures the saturation curve $x_{\rm sat} = x(P)$ has a maximum at around $x_m = 9.5\%$,[12] for $x > x_m$ the drop barrier always remains finite. This can be seen in Fig. 4, and indicates that the functional of Ref. 11 is

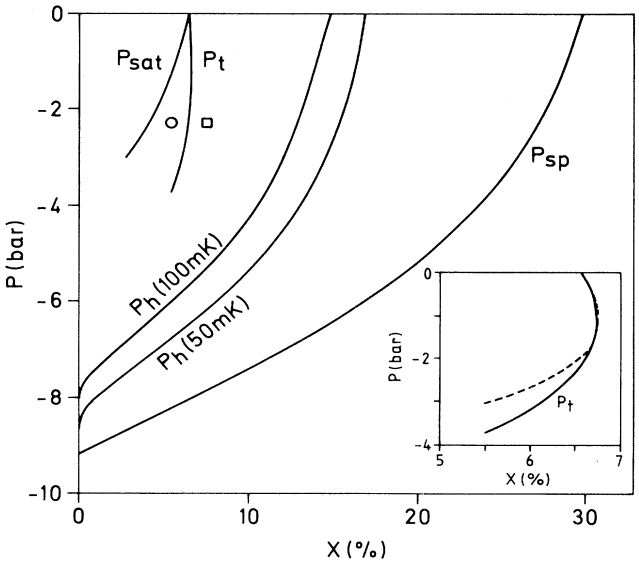

FIG. 5. Transition pressure P_t from bubble to drop nucleation and homogeneous nucleation pressure P_h for T =50 and 100 mK, as functions of ^{3}He concentration. Also shown are the saturation $P_{\rm sat}$ and spinodal $P_{\rm sp}$ curves. In the lower right-hand corner we show again P_t (solid line) and compare it with the result obtained in the capillarity approximation (dashed line).

able to reproduce, at least qualitatively, this experimental fact.

The phase diagram of the mixture at $T = 0$ in the (P,x) plane is represented in Fig. 5 for negative pressures. The saturation curve is labeled as $P_{\rm sat}(x)$, and the spinodal line as $P_{\rm sp}(x)$ (see also Fig. 1 of Ref. 4). Also shown is the $P_t(x)$ line. Phase transition will be driven by bubble nucleation on the left of that line, and by drop nucleation on the right. The configurations displayed in Figs. 2 and 3 are represented by a circle and a square, respectively. For pressures below ~ -3.8 bar, no genuine bubble configurations can be found in the mixture, and only ^{3}He-rich drops are present as nucleation clusters.

In the lower right-hand corner of Fig. 5 we display on a magnified scale the $P_t(x)$ curve and compare the capillarity (dashed line) with the density-functional result. As expected, the capillarity approach is a good approximation only near saturation, i.e., zero pressure and concentrations close to 6.6%. It is interesting to note that P_t exists for concentrations slightly higher than the saturation value at P =0, and that it is a bivaluate function of x.

C. Homogeneous nucleation pressure

The nucleation rate, i.e., the number of nuclei formed in the homogeneous system per unit of time and of volume due to thermal fluctuations is given by

$$J_T = J_{0T} \exp^{-\Delta\Omega/kT}, \tag{9}$$

where k is the Boltzmann's constant and the preexponential factor J_{0T} depends on the dynamics of the nucleation process. To make a quantitative estimate of the homogeneous nucleation pressure P_h, one may proceed as in Refs. 13 and 14, that is, consider a rate $J_T = 1$ cm^{-3} sec^{-1} and solve the equation

$$\frac{\Delta\Omega}{kT} = \ln J_{0T}\ ({\rm cm}^{-3}\,{\rm sec}^{-1}), \tag{10}$$

taking for $J_{0T} \sim 2 \times 10^{33}$ cm^{-3} sec^{-1} as in Ref. 14, and using the lower barrier height $\Delta\Omega$ that corresponds to either bubble or drop configuration. P_h is displayed in Fig. 5 as a function of x for 50 and 100 mK temperature. Notice that at a temperature as low as 50 mK, P_h differs appreciably from $P_{\rm sp}$ even at low ^{3}He concentrations. This is again a manifestation of the presence of ^{3}He surface states (Andreev states), see also Fig. 5 of Ref. 4.

V. SUMMARY

In a series of works (Refs. 4, 16, and the present work), we have carried out a detailed study of thermal nucleation and cavitation in ^{3}He-^{4}He liquid mixtures at low temperatures using a density-functional approach that overcomes the shortcomings inherent in the capillarity model usually employed in classical nucleation theory.

The flexibility of the density-functional approach is especially indicated for helium mixtures, where the limited miscibility of both isotopes at low temperatures and the existence of surface Andreev states make the shape of the nucleation clusters hard to guess and mimick by means of simple sharp-surface models.

We have quantitatively shown the influence of even low ^{3}He concentrations on the cavitation tensile strength, and studied the bubble-to-drop nucleation transition at concentrations above saturation. The experimental knowledge of cavitation in liquid helium is rather scarce, even in the best studied case of pure ^{4}He, and it is still a subject of debate (see Ref. 15 and references therein).

At positive pressures and supersaturated mixtures, we have argued about the possibility of vortices with cores rich in ^{3}He as nucleation sites to conciliate theory and experiment.[16] At negative pressures, the influence of vortices on cavitation in pure ^{4}He has been studied in detail by Maris.[17] A systematic investigation of the effect of vortices on cavitation and nucleation in liquid-helium mixtures using a realistic density functional is called for in order to put the theoretical estimates on firmer ground.

ACKNOWLEDGMENTS

This work has been supported by DGICYT (Spain) Grants No. PB92-0761 and PB92-0820. M.G. thanks the Departament d'Ensenyament of the Generalitat de Catalunya, for financial support. We thank the generous computer support of the CESCA facility.

[1] K. Binder, in *Material Science and Technology*, edited by R.W. Cahn, P. Haasen, and E.J. Kramer (VCH, Weinheim, Germany, 1991), Vol. 5.
[2] D.W. Oxtoby, in *Fundamentals of Inhomogeneous Liquids*, edited by D. Henderson (Dekker, New York, 1992), Chap. 10, p. 407.
[3] X.C. Zeng and D.W. Oxtoby, J. Chem. Phys. **95**, 5940 (1991).
[4] M. Guilleumas, D.M. Jezek, M. Pi, M. Barranco, and J. Navarro, Phys. Rev. B **51**, 1140 (1995).
[5] I.M. Lifshitz and Yu. Kagan, Zh. Eksp. Teor. Fiz. **62**, 385 (1972) [Sov. Phys. JETP **35**, 206 (1972)].
[6] I.M. Lifshitz, V.N. Polesskii, and V.I. Khokhlor, Zh. Eksp. Teor. Fiz. **74**, 268 (1978) [Sov. Phys. JETP **47**, 137 (1978)].
[7] K. Nishioka and I. Kusaka, J. Chem. Phys. **96**, 5370 (1992).
[8] M. A. Solís and J. Navarro, Phys. Rev. B **45**, 13 080 (1992).
[9] M. Guilleumas, M. Pi, M. Barranco, J. Navarro, and M. A. Solís, Phys. Rev. B **47**, 9116 (1993).
[10] F. Dalfovo and S. Stringari, Phys. Lett. A **112**, 171 (1985).
[11] F. Dalfovo, Ph.D. thesis, University of Trento, 1989.
[12] C. Ebner and D.O. Edwards, Phys. Rep. **2**, 77 (1970).
[13] Q. Xiong and H.J. Maris, J. Low Temp. Phys. **77**, 347 (1989).
[14] D.M. Jezek, M. Guilleumas, M. Pi, M. Barranco, and J. Navarro, Phys. Rev. B **48**, 16 582 (1993).
[15] M.S. Pettersen, S. Balibar, and H.J. Maris, Phys. Rev. B **49**, 12 062 (1994).
[16] D.M. Jezek, M. Guilleumas, M. Pi, and M. Barranco, Phys. Rev. B **51**, 11 981 (1995).
[17] H. J. Maris, J. Low Temp. **94**, 125 (1994).